Missouri University of Science and Technology
Scholars' Mine

Chemistry Faculty Research & Creative Works | Chemistry

01 Sep 2022

Crystal Structure, Electronic Structure, and Optical Properties of the Novel Li4cdge2s7, a Wide-Bandgap Quaternary Sulfide with a Polar Structure Derived from Lonsdaleite

Andrew J. Craig

Seung Han Shin

Jeong Bin Cho

Srikanth Balijapelly

et. al. For a complete list of authors, see https://scholarsmine.mst.edu/chem_facwork/3177

Follow this and additional works at: https://scholarsmine.mst.edu/chem_facwork

Part of the Chemistry Commons

Recommended Citation

A. J. Craig and S. H. Shin and J. B. Cho and S. Balijapelly and J. C. Kelly and S. S. Stoyko and A. Choudhury and J. I. Jang and J. A. Aitken and A. Sarjeant, "Crystal Structure, Electronic Structure, and Optical Properties of the Novel Li4cdge2s7, a Wide-Bandgap Quaternary Sulfide with a Polar Structure Derived from Lonsdaleite," *Acta Crystallographica Section C: Structural Chemistry*, vol. 78, no. Pt 9, pp. 470 - 480, International Union of Crystallography; Wiley, Sep 2022.
The definitive version is available at https://doi.org/10.1107/S2053229622008014

This Article - Journal is brought to you for free and open access by Scholars' Mine. It has been accepted for inclusion in Chemistry Faculty Research & Creative Works by an authorized administrator of Scholars' Mine. This work is protected by U. S. Copyright Law. Unauthorized use including reproduction for redistribution requires the permission of the copyright holder. For more information, please contact scholarsmine@mst.edu.

Check for updates

Acta Cryst C STRUCTURAL CHEMISTRY

ISSN 2053-2296

Crystal structure, electronic structure, and optical properties of the novel $Li_4CdGe_2S_7$, a wide-bandgap quaternary sulfide with a polar structure derived from lonsdaleite

Andrew J. Craig,[a] Seung Han Shin,[b] Jeong Bin Cho,[b] Srikanth Balijapelly,[c] Jordan C. Kelly,[a] Stanislav S. Stoyko,[a] Amitava Choudhury,[c] Joon I. Jang[b]* and Jennifer A. Aitken[a]*

[a]Department of Chemistry and Biochemistry, Duquesne University, Pittsburgh, PA 15282, USA, [b]Department of Physics, Sogang University, 35 Baekbeom-ro, Mapo-gu, Seoul 04107, Republic of Korea, and [c]Department of Chemistry, Missouri University of Science and Technology, Rolla, MO 65409, USA. *Correspondence e-mail: jjcoupling@sogang.ac.kr, aitkenj@duq.edu

Received 30 June 2022
Accepted 8 August 2022

Edited by A. Sarjeant, Bristol-Myers Squibb, USA

Keywords: crystal structure; thiogermanate; diamond-like; wide bandgap; lonsdaleite; quaternary sulfide.

CCDC reference: 2195746

Supporting information: this article has supporting information at journals.iucr.org/c

The novel quaternary thiogermanate $Li_4CdGe_2S_7$ (tetralithium cadmium digermanium heptasulfide) was discovered from a solid-state reaction at 750 °C. Single-crystal X-ray diffraction data were collected and used to solve and refine the structure. $Li_4CdGe_2S_7$ is a member of the small, but growing, class of I_4–II–IV_2–VI_7 diamond-like materials. The compound adopts the $Cu_5Si_2S_7$ structure type, which is a derivative of lonsdaleite. Crystallizing in the polar space group *Cc*, $Li_4CdGe_2S_7$ contains 14 crystallographically unique ions, all residing on general positions. Like all diamond-like structures, the compound is built of corner-sharing tetrahedral units that create a relatively dense three-dimensional assembly. The title compound is the major phase of the reaction product, as evidenced by powder X-ray diffraction and optical diffuse reflectance spectroscopy. While the compound exhibits a second-harmonic generation (SHG) response comparable to that of the $AgGaS_2$ (AGS) reference material in the IR region, its laser-induced damage threshold (LIDT) is over an order of magnitude greater than AGS for λ = 1.064 µm and τ = 30 ps. Bond valence sums, global instability index, minimum bounding ellipsoid (MBE) analysis, and electronic structure calculations using density functional theory (DFT) were used to further evaluate the crystal structure and electronic structure of the compound and provide a comparison with the analogous I_2–II–IV–VI_4 diamond-like compound Li_2CdGeS_4. $Li_4CdGe_2S_7$ appears to be a better IR nonlinear optical (NLO) candidate than Li_2CdGeS_4 and one of the most promising contenders to date. The exceptional LIDT is likely due, at least in part, to the wider optical bandgap of ~3.6 eV.

1. Introduction

Diamond-like materials are those whose structures are based on a closest-packed array of anions with the cations filling half of the tetrahedral holes. There are two types of closest packing: cubic closest packing, which is the most common structure for diamonds, and hexagonal closest packing, which is more rarely encountered. Hexagonal diamond is named after the legendary crystallographer Professor Kathleen Lonsdale (Frondel & Marvin, 1967; Bundy & Kasper, 1967). This form of diamond was first discovered in 1967 in high-pressure laboratory studies and at about the same time in nature at the Canyon Diablo iron meteorite site, where it was believed to have been created by the high pressure of the impact. Londaleite has since been identified in other geographical locations, for example, in impact melts from the Ries

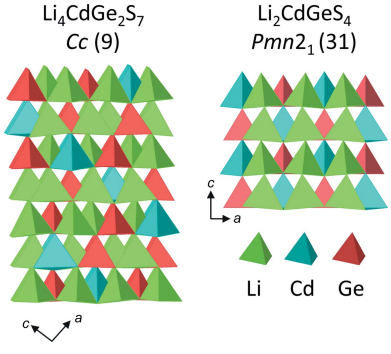

s20532296, 2022, 9, Downloaded from https://onlinelibrary.wiley.com/doi/10.1107/S2053229622008014 by Missouri University Of Science, Wiley Online Library on [21/02/2023]. See the Terms and Conditions (https://onlinelibrary.wiley.com/terms-and-conditions) on Wiley Online Library for rules of use; OA articles are governed by the applicable Creative Commons License

crater in southern Germany (Hough *et al.*, 1995). There was some controversy surrounding the enigmatic londsdaleite for some time. However, researchers have observed, *via* ultrafast *in-situ* X-ray diffraction studies, the transition from pyrolytic graphite to lonsdaleite *via* shock compression at pressures exceeding 170 GPa (Kraus *et al.*, 2016). While the hexagonal form of diamond needs special conditions of high pressure to form, derivatives of this structure can be found in many common minerals, for example, wurtzite (Friedel, 1861), greenockite (Ulrich & Zachariasen, 1925), and enargite (Breithaupt & Plattner, 1850; Pauling & Weinbaum, 1934).

Compounds with diamond-like structures are called 'normal valence compounds' and follow basic valence electron rules and Pauling's principles (Pauling, 1929; Goryunova, 1965; Parthé, 1964; Pamplin, 1981). The average number of valence electrons, VE_{ave}, and valence electrons per anion, VE_A, should be four and eight, respectively. The total number of valence electrons for all ions in the formula unit is represented as ve_{total} and n is the number of ions or anions as seen in Equations (1) and (2) (Parthé, 1964; Goryunova, 1965).

$$VE_{ave} = ve_{total}/n_{ions} \quad (1)$$

$$VE_A = ve_{total}/n_{anions} \quad (2)$$

These principles allow for the prediction of all possible diamond-like compounds (Parthé, 1964; Goryunova, 1965; Pamplin, 1981). Several formulae are predicted for compounds that follow the above rules and possess local charge neutrality. For example, synthetic investigations into quaternary derivatives of the diamond structure began in earnest in the 1960s by several groups, mainly focused on compounds of the I_2–II–IV–VI_4 formula. These formulae are generally expressed by using Roman numerals to indicate the valence of the ions and the subscript provides the number of those ions per formula unit. However, based on the rules outlined above, other quaternary formulae are possible when local charge neutrality is not maintained, as in the I_4–II–IV_2–VI_7 family of compounds that were first reported in 1980 (Schäfer *et al.*, 1980). These compounds, with crystal structures related to either cubic diamond (*C*2) or lonsdaleite (*Cc*), are valence precise, *i.e.* charge balanced; yet, the local charge is not satisfied for all of the anions in the structure and thus, as predicted by Pauling's second rule, the structures are less regular and feature subtle distortions of the respective tetrahedral units.

Table 1 lists all of the known I_4–II–IV_2–VI_7 compounds. Two of these compounds, $Li_4MnGe_2S_7$ and $Li_4MnSn_2Se_7$, have been proposed as potential anode materials for Li-ion batteries; they possess specific capacities of 585 and 725 mAh g^{-1}, respectively, exceeding the theoretical capacity of 372 mAh g^{-1} for commercial-grade graphite, while exhibiting excellent cycling stability after 50 cycles with values of 450 and 660 mAh g^{-1}, respectively (Kaib *et al.*, 2013). Other I_4–II–IV_2–VI_7 compounds have been investigated for their potential as nonlinear optical (NLO) materials in the IR regime. $Li_4MgGe_2S_7$ boasts the widest optical bandgap among the known I_4–II–IV_2–VI_7 members, 4.12 eV, and a good phase-matching (PM) second-harmonic generation (SHG) response of 0.7 × $AgGaS_2$ (AGS) at λ = 2.09 µm, and a significant laser-induced damage threshold (LIDT) of 7 × AGS (λ = 1.064 µm, pulse width, τ, = 10 ns) (Abudurusuli *et al.*, 2021). $Li_4HgGe_2S_7$, with a narrower optical bandgap of 2.75 eV, has a stronger SHG response of 1.5 × AGS at λ = 2.09 µm, but a lower LIDT, 3.5 × AGS (λ = 1.064 µm, τ = 50 ns) (Wu *et al.*, 2017). $Li_4HgSn_2Se_7$ possesses an even narrower bandgap of 2.10 eV, and exhibits a greater PM SHG response of 3.6 × AGS at λ = 2.09 µm (Guo *et al.*, 2019). While $Cu_4ZnGe_2Se_7$ displays a very weak SHG response (Sinagra *et al.*, 2021), $Cu_4MnGe_2S_7$ has a second-order NLO susceptibility, $\chi^{(2)}$, of 2.33 ± 0.86 pm V^{-1}, assessed at the static limit (Glenn *et al.*, 2021). Recently, we have demonstrated that $Li_4CdSn_2S_7$ is the best I_4–II–IV_2–VI_7 IR–NLO candidate material to date, with an excellent balance of properties, an optical bandgap of 2.59 eV, an exceptional LIDT of 12.5 × AGS (λ = 1.064 µm, τ = 30 ps), and a $\chi^{(2)}$ value of 35 pm V^{-1} at the static limit (Zhang, Stoyko *et al*, 2020). This material has the potential to surpass the benchmark AGS and $AgGaSe_2$ (AGSe) in difference frequency generation applications in the mid-IR.

Considering the sparse number of I_4–II–IV_2–VI_7 compounds and their attractive physicochemical properties, we sought to expand this class of materials. In this work, we chose lithium as the monovalent ion because Li-containing sulfides generally have wider bandgaps and corresponding greater LIDTs compared to the analogous Cu- and Ag-containing phases. The relatively large and polarizable Cd was selected as the divalent metal due to the number of Cd-containing compounds with strong SHG, for example, diamond-like CdS and CdSe (Jackson *et al.*, 1997; Cheng *et al.*, 2019). We picked sulfur as the hexavalent ion because sulfides usually have the widest bandgaps in a series of chalcogenides, further increasing the odds of obtaining a material with a high LIDT. As the tin-containing compound, discussed above, had already been discovered and found to possess outstanding IR–NLO properties, we turned our attention to the next smallest tetrel and targeted the new compound $Li_4CdGe_2S_7$. Our efforts were successful, as here we report the synthesis, crystal structure, and optical bandgap of $Li_4CdGe_2S_7$. NLO property measurements in the IR region for an ungraded sample of this compound indicate a similar performance to the outstanding $Li_4CdSn_2S_7$ and a better performance than the analogous I_2–II–IV–VI_4 material Li_2CdGeS_4. Bond valence sums, global instability index, minimum bounding ellipsoid calculations, and electronic structure calculations performed using density functional theory (DFT) were carried out for both diamond-like compounds in the Li–Cd–Ge–S system to reveal their subtle structural differences.

2. Experimental

2.1. Reagents

Powders of lithium sulfide (Li_2S) (99.9%, Cerac), cadmium metal (99.999%, Strem), and sublimed sulfur (99.5%, Fisher Scientific) were used as obtained and without further purification. Chunks of germanium metal (99.999%, Strem) were

s20532296, 2022, 9, Downloaded from https://onlinelibrary.wiley.com/doi/10.1107/S2053229622008014 by Missouri University Of Science, Wiley Online Library on [21/02/2023]. See the Terms and Conditions (https://onlinelibrary.wiley.com/terms-and-conditions) on Wiley Online Library for rules of use; OA articles are governed by the applicable Creative Commons License

Table 1
Known I_4–II–IV_2–VI_7 diamond-like compounds with structures derived from cubic diamond (*C*2) or lonsdaleite (*Cc*) with the corresponding SHG responses and optical bandgaps where applicable.

Compound	Space group	SHG response†	E_g (eV)	Reference
$Li_4MgGe_2S_7$	*Cc*	0.7 × AGS (λ = 2.09 µm)	4.12	Abudurusuli *et al.* (2021)
$Li_4MnGe_2S_7$	*Cc*			Kaib *et al.* (2013)
$Li_4MnSn_2Se_7$	*Cc*			Kaib *et al.* (2013)
$Li_4CdGe_2S_7$	*Cc*	∼1 × AGS (λ = 1.8 µm)	3.6	This work
$Li_4CdSn_2S_7$	*Cc*	$\chi^{(2)}$ = 35.0 ± 3.5 pm V^{-1}	2.59	Zhang, Stoyko *et al.* (2020)
$Li_4HgGe_2S_7$	*Cc*	1.5 × AGS (λ = 2.09 µm)	2.75	Wu *et al.* (2017)
$Li_4HgSn_2S_7$	*Cc*			Aitken (2001)
$Li_4HgSn_2Se_7$	*Cc*	3.6 × AGS (λ = 2.09 µm)	2.1	Guo *et al.* (2019)
$Ag_4CdGe_2S_7$	*Cc*			Gulay *et al.* (2002)
$Ag_4HgGe_2S_7$	*Cc*			Gulay *et al.* (2002)
$Cu_4MnGe_2S_7$	*Cc*	$\chi^{(2)}$ = 2.33 × 0.86 pm V^{-1}	1.98	Glenn *et al.* (2021)
$Cu_4FeGe_2S_7$	*C*2			Craig *et al.* (2020)
$Cu_4CoGe_2S_7$	*C*2			Craig *et al.* (2020)
$Cu_4NiSi_2S_7$	*C*2			Schäfer *et al.* (1980)
$Cu_4NiGe_2S_7$	*C*2			Schäfer *et al.* (1980)
$Cu_4ZnGe_2Se_7$	*C*2	weak	0.91	Sinagra *et al.* (2021)

† $\chi^{(2)}$ values are assessed at the static limit, where the sample and the reference are phase matching and multiphoton absorption is not a factor.

ground to a fine powder in an argon-filled glovebox using a Diamonite mortar and pestle prior to use. All reagents were stored in an inert-atmosphere glovebox.

2.2. Synthesis and crystallization

$Li_4CdGe_2S_7$ was prepared by high-temperature, solid-state synthesis. Stoichiometric quantities of the elemental reagents and a 10% excess of Li_2S were weighed in an argon-filled glovebox before being briefly ground together in an agate mortar and pestle. This mixture was then placed in a loosely capped graphite tube that was next loaded into a 12 mm o.d. fused-silica tube that was flame-sealed under ∼10^{-3} mbar pressure before being placed in a programmable box furnace. The sample was heated to 800 °C in 12 h and allowed to dwell at this temperature for 120 h. After this, the reaction was cooled to 600 °C over 100 h before being allowed to return ambiently to room temperature over 24 h. The reaction vessel was opened and the product was stored in the glovebox because it was deemed to be somewhat air/moisture sensitive. An optical microscope was used to inspect the product for single crystals suitable for X-ray diffraction analysis. A portion of this sample was used for NLO measurements, while the rest of the sample was ground and stored in a desiccator for further characterization.

2.3. Single-crystal X-ray diffraction and structure refinement

A colorless crystal was affixed to a glass fiber with cyanoacrylate glue. Single-crystal X-ray diffraction data were collected at room temperature with a Bruker APEXII CCD single-crystal X-ray diffractometer using Mo *Kα* radiation, λ = 0.71073 Å. Selected crystallographic data, data collection and structure refinement details are given in Table 2. Extinction was refined for this structure and the Flack parameter (Flack & Bernardinelli, 1999) was refined to 0.001 (5). The largest peak and deepest hole in the difference Fourier map, 0.269 and −0.210 e Å^{-3}, were located 1.09 Å from Ge2 and 2.13 Å from Li4, respectively. Figures depicting the crystal structure were created using *CrystalMaker* (Palmer, 2019) and the resulting crystallographic information file (CIF).

Table 2
Experimental details.

Crystal data	
Chemical formula	$Li_4CdGe_2S_7$
M_r	509.76
Crystal system, space group	Monoclinic, *Cc*
Temperature (K)	293
a, *b*, *c* (Å)	16.8354 (10), 6.7870 (4), 10.1499 (6)
β (°)	93.710 (3)
V (Å^3)	1157.32 (12)
Z	4
Radiation type	Mo *Kα*
μ (mm^{-1})	8.18
Crystal size (mm)	0.21 × 0.12 × 0.11
Data collection	
Diffractometer	Bruker SMART APEXII
Absorption correction	Multi-scan (*SADABS*; Sheldrick, 2002)
T_{min}, T_{max}	0.549, 0.747
No. of measured, independent and observed [$I > 2\sigma(I)$] reflections	7415, 2634, 2612
R_{int}	0.017
$(\sin \theta/\lambda)_{max}$ (Å^{-1})	0.649
Refinement	
$R[F^2 > 2\sigma(F^2)]$, $wR(F^2)$, S	0.010, 0.024, 1.08
No. of reflections	2634
No. of parameters	129
No. of restraints	2
$\Delta\rho_{max}$, $\Delta\rho_{min}$ (e Å^{-3})	0.27, −0.21
Absolute structure	Refined as an inversion twin
Absolute structure parameter	0.001 (5)

Computer programs: *APEX2* (Bruker, 2010), *SMART* (Bruker, 2010), *SHELXT* (Sheldrick, 2015*a*), *SHELXL2018* (Sheldrick, 2015*b*), and *CrystalMaker* (Palmer, 2019).

2.4. Powder X-ray diffraction

The microcrystalline sample was ground well and deposited onto a zero-background silicon wafer. Powder X-ray diffraction data were collected using a Malvern Panalytical Empyrean 3 multipurpose powder X-ray diffractometer with an X'cellerator detector operating in Bragg–Brentano geometry and using Cu *Kα* radiation, λ = 1.541871 Å. The tube was energized using 45 kV and 40 mA. Data were collected from 5 to 100° 2*θ* in steps of 0.0167° at a scan speed of 0.023537° s^{-1}. A 0.04 rad soller slit and a 2° anti-scatter slit were used on the incident side of the beam, while the diffracted beam optics consisted of a 0.04 rad soller slit, a programmable anti-scatter slit, and a nickel filter. Phase identification of crystalline components was carried out using the *X'Pert HighScore Plus* (Degen *et al.*, 2014) software package and the International Centre for Diffraction Data (ICDD) powder diffraction file (PDF) database (Smith & Jenkins, 1996).

s20532296, 2022, 9, Downloaded from https://onlinelibrary.wiley.com/doi/10.1107/S2053229622008014 by Missouri University Of Science, Wiley Online Library on [21/02/2023]. See the Terms and Conditions (https://onlinelibrary.wiley.com/terms-and-conditions) on Wiley Online Library for rules of use; OA articles are governed by the applicable Creative Commons License

2.5. Optical diffuse reflectance UV–Vis–NIR spectroscopy

A Varian Cary 5000 UV–Vis–NIR spectrophotometer coupled with a diffuse reflectance accessory was used to collect data from 2500 to 200 nm at a rate of 600 nm min^{-1}. The 100% reflectance standard was $BaSO_4$ (Fisher Scientific, 99.92%). The sample was ground and pressed on top of the reference that was preloaded in the sample cup. Reflectance data were converted to absorption by employing the Kubelka–Munk equation (Kubelka & Munk, 1931) and plotted as a function of energy. The optical bandgap was estimated by extrapolation of the absorption edge to the baseline.

2.6. Nonlinear optical characterization

A microcrystalline sample of $Li_4CdGe_2S_7$ enclosed in a fused-silica capillary tube was provided for NLO characterization to assess SHG and the LIDT. It should be noted that this was an ungraded sample, *i.e.* the sample was not sieved into discrete particle size ranges. Determination of SHG dependence on particle size is necessary to assess phase matching; however, due to the fact that the sample containing the title compound is not phase pure, phase-matching results would likely be inaccurate. The absolute value of the SHG coefficient, together with the phase-matching behavior, will be determined for the title compound when phase-pure samples are obtained. The SHG measurements were carried out at room temperature using an input wavelength, λ, ranging from 1.0 to 1.8 µm. The LIDT was assessed at 1.064 µm based on the intensity dependence of the SHG response. Coherent light with a wavelength of 1.064 µm was initially produced using an EKSPLA PL-2250 series diode-pumped Nd:YAG laser with a pulse width (τ) of 30 ps and a repetition rate of 50 Hz to generate tunable pulses. The Nd:YAG laser pumped an EKSPLA Harmonics Unit (HU) H400 in which the input beam was frequency tripled to 0.355 µm by a series of NLO beam mixing. Two beams of 0.355 and 1.064 µm then entered an EKSPLA PG403-SH-DFG Optical Parametric Oscillator (OPO) composed of four main parts: (i) a double-pass parametric generator, (ii) a single-pass parametric amplifier, (iii) a second-harmonic (SH) generator, and (iv) a difference-frequency generator (DFG). A detailed description of our laser and detection setup can be found elsewhere (Zhang, Stoyko *et al.*, 2020). The sample was compared to an optical-quality reference NLO material, AGS, from Gooch and Housego (Ohio) LLC. The reference, obtained as a commercial-grade single crystal, was ground to a powder for measurements.

2.7. Electronic structure calculations

Electronic band structure calculations were carried out using first principles at a DFT level using the *Quantum Espresso* plane-wave (PW) based software package (Giannozzi *et al.*, 2009). The revised Perdew–Burke–Ernzerhof generalized gradient approximation (PBESol) (Perdew *et al.*, 1996, 2008) was employed and the projected augmented wave (PAW) pseudopotential was used to describe the effect of the core electrons with the following states treated as valence states: 3*s* and 3*p* for S, 4*s* and 4*p* for Ge, 5*s*, 4*p*, and 4*d* for Cd, and 2*s* for Li. A kinetic-energy cutoff of 544 eV and a Monkhorst–Pack (Monkhorst & Pack, 1976) *k*-point grid size of 5 × 4 × 4 was used for Brillouin zone integration. The total

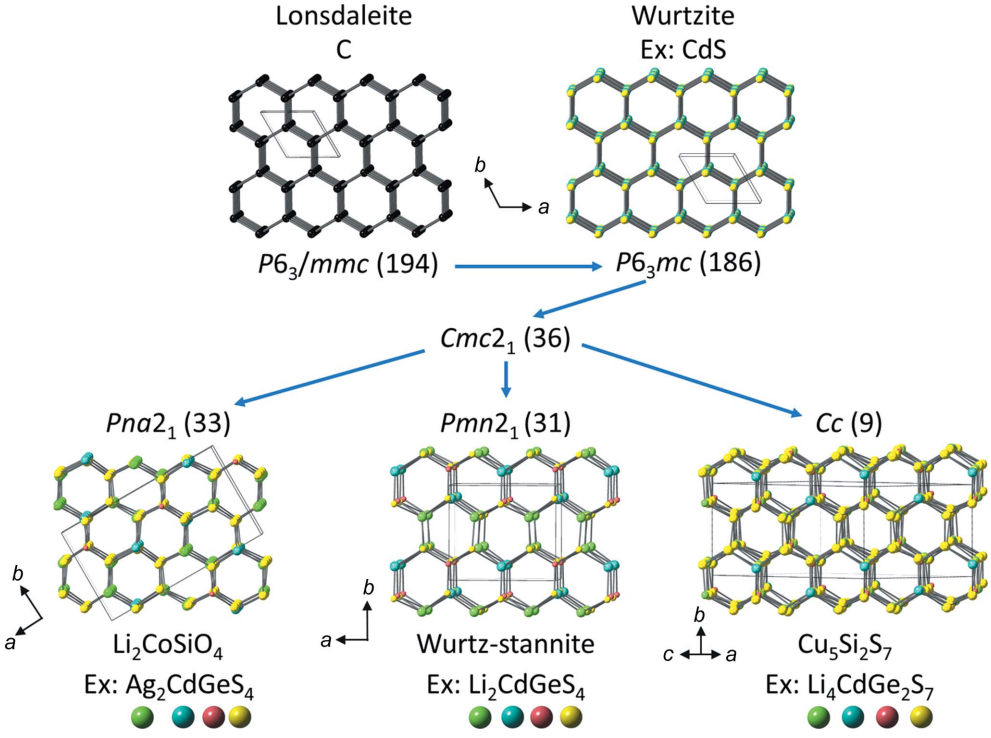

Figure 1
Derivation of some diamond-like structures from that of hexagonal diamond, lonsdaleite, with blue arrows showing group–subgroup relationships.

s20532296, 2022, 9, Downloaded from https://onlinelibrary.wiley.com/doi/10.1107/S2053229622008014 by Missouri University Of Science, Wiley Online Library on [21/02/2023]. See the Terms and Conditions (https://onlinelibrary.wiley.com/terms-and-conditions) on Wiley Online Library for rules of use; OA articles are governed by the applicable Creative Commons License

energy convergence threshold of 10^{-6} eV was used. The structure was fully relaxed until the force on each atom was below 0.01 eV Å^{-1}. The density of states was calculated using a Gaussian smearing of 0.05 eV.

3. Results and discussion

3.1. Crystal structure

The title compound, $Li_4CdGe_2S_7$, crystallizes in the polar space group *Cc* (No. 9) and adopts the $Cu_5Si_2S_7$ structure type (Table 2) (Dogguy *et al.*, 1982). *Via* group–subgroup relationships, this crystal structure can be considered a derivative of the hexagonal form of diamond, *i.e.* lonsdaleite (Fig. 1), where each atom in the formula unit occupies a crystallographically-unique general position in the structure. With the increase in the number of elements from the parent diamond structure to the title compound, a decrease in symmetry and a larger unit cell are observed. The 'honeycomb' pattern seen in all DLSs, regardless of these structural distortions, is evident in this structure and can be seen in Fig. 1. The noncentrosymmetric nature of the structure is obvious when visualized along the crystallographic *b* axis (Fig. 2, left); all metal–sulfur tetrahedra are unidirectionally aligned. Among the corner-sharing tetrahedra, there are adjacent GeS_4 tetrahedra that form $[Ge_2S_7]^{6-}$ subunits. The structures for the compounds of the I_4–II–IV_2–VI_7 stoichiometry exhibit a more complex cation ordering pattern than that seen in the diamond-like I_2–II–IV–VI_4 compounds. Fig. 2 (right) compares the title compound to its analogous I_2–II–IV–VI_4 phase Li_2CdGeS_4 (Lekse *et al.*, 2009).

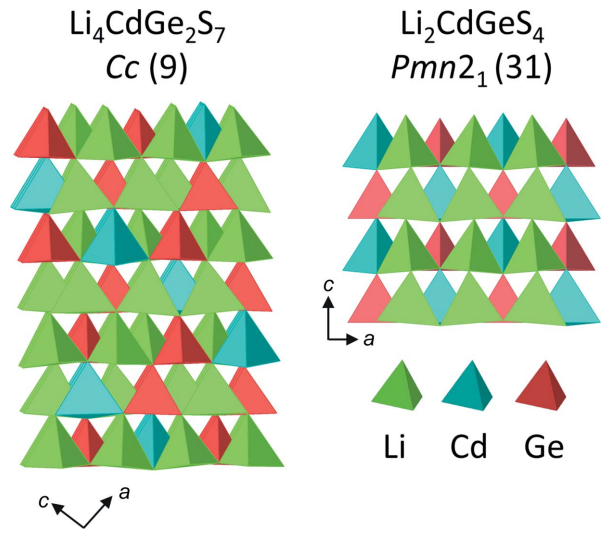

Figure 2
Polyhedral representation of $Li_4CdGe_2S_7$ compared to Li_2CdGeS_4. The alignment of all tetrahedral units along one crystallographic direction renders the structures noncentrosymmetric and capable of producing SHG.

As explained previously, the features of diamond-like compounds can be generally rationalized using Pauling's tenets with the second and fourth being most pertinent to the discussion of $Li_4CdGe_2S_7$ and its comparison to Li_2CdGeS_4. The second rule, *i.e.* the electrostatic valence principle, states that the charge of the anions should be balanced by cations within the first coordination sphere in order for that coordination environment to be considered 'regular' (Pauling, 1929). This is the case for all anions within the structure of Li_2CdGeS_4; however, local charge neutrality is not completely achieved in $Li_4CdGe_2S_7$, as demonstrated in the extended connectivity table (Table 3) (Parthé, 1996). Each sulfur anion bears a −2 charge and each cation it is bound to contributes $\frac{1}{4}$ of its positive charge to that particular coordination polyhedron (Table 3). While S1, S2, S6, and S7 are locally charge compensated, each being bound to two Li, one Cd, and one Ge, S3 and S5 are undercompensated with respect to charge and the charge of S4 is overcompensated. Both S3 and S5 are bound to three Li and one Ge,

Table 3
Extended connectivity table for $Li_4CdGe_2S_7$ used to predict structural distortions in accordance with Pauling's second rule.

		Anions							Horizontal Bond Strength Sums
		S1	S2	S3	S4	S5	S6	S7	
Cations	Li1		$\frac{1}{4}$	$\frac{1}{4}$	$\frac{1}{4}$	$\frac{1}{4}$			Σ = 1
	Li2	$\frac{1}{4}$				$\frac{1}{4}$	$\frac{1}{4}$	$\frac{1}{4}$	Σ = 1
	Li3	$\frac{1}{4}$	$\frac{1}{4}$	$\frac{1}{4}$				$\frac{1}{4}$	Σ = 1
	Li4			$\frac{1}{4}$	$\frac{1}{4}$	$\frac{1}{4}$	$\frac{1}{4}$		Σ = 1
	Cd	$\frac{2}{4}$	$\frac{2}{4}$				$\frac{2}{4}$	$\frac{2}{4}$	Σ = 2
	Ge1	$\frac{4}{4}$	$\frac{4}{4}$	$\frac{4}{4}$	$\frac{4}{4}$				Σ = 4
	Ge2				$\frac{4}{4}$	$\frac{4}{4}$	$\frac{4}{4}$	$\frac{4}{4}$	Σ = 4
Vertical Bond Strength Sums		Σ = 2	Σ = 2	Σ = 1.75	Σ = 2.5	Σ = 1.75	Σ = 2	Σ = 2	
Charge compensation*		CMP	CMP	UNDER CMP	OVER CMP	UNDER CMP	CMP	CMP	

* CMP = compensated.

s20532296, 2022, 9, Downloaded from https://onlinelibrary.wiley.com/doi/10.1107/S2053229622008014 by Missouri University Of Science, Wiley Online Library on [21/02/2023]. See the Terms and Conditions (https://onlinelibrary.wiley.com/terms-and-conditions) on Wiley Online Library for rules of use; OA articles are governed by the applicable Creative Commons License

such that the corresponding tetrahedra hold a local charge of −0.25. On the other hand, S4 is bound to two Li and two Ge, which overcompensates the local charge by +0.5. As a result of these local charge imbalances, the structure slightly distorts, as forecasted by Pauling (1929) and evident from the bond distances and angles displayed in Tables 4 and 5.

All of the metal–sulfur bond distance ranges are wider for the title compound than those observed in the corresponding I_2–II–IV–VI_4 compound, while the average metal–sulfur bond distances for each type of cation are identical. These average Li—S, Cd—S, and Ge—S bond distances are comparable to those found in other diamond-like materials, for example, α-Li_2ZnGeS_4 (Zhang, Clark *et al.*, 2020), β-Li_2ZnGeS_4 (Huang *et al.*, 2019), Li_2CoGeS_4 (Brant *et al.*, 2015), Ag_2CdGeS_4 (Brunetta *et al.*, 2012), and Cu_2CdGeS_4 (Parasyuk *et al.*, 2005). With the slight charge undercompensation present for S3 and S5, one would expect some shortening of the *M*—S bond distances. However, it should be noted that not all *M*—S bonds involving these anions are the shortest; yet the shortest Ge1 and Ge2 distances to sulfur exist for S3 and S5, respectively. The charge overcompensation existing for S4 is double the magnitude of the undercompensation for S3 and S5, and, therefore, the distortion is more apparent for S4. The cation–sulfur bonds containing S4 are the longest in each of their respective tetrahedra. Similar subtle structural distortions have been observed in other I_4–II–IV_2–VI_7 compounds, for example, $Cu_4FeGe_2S_7$, $Cu_4CoGe_2S_7$, $Li_4CdSn_2S_7$, $Cu_4MnGe_2S_7$, and $Cu_4ZnGe_2Se_7$ (Craig *et al.*, 2020; Zhang, Stoyko *et al.*, 2020; Glenn *et al.*, 2021; Sinagra *et al.*, 2021).

The structural distortions are also present in the bond angles of the title compound (Table 5). The average tetrahedral bond angles in both $Li_4CdGe_2S_7$ and Li_2CdGeS_4 are, within estimated standard deviations, identical to one another and the ideal value for tetrahedra. The bond angle ranges for the tetrahedra in $Li_4CdGe_2S_7$ are broader than those found in Li_2CdGeS_4. For example, the S—Li—S bond angles in $Li_4CdGe_2S_7$ range from 101.4 (3) to 115.7 (4)°, while those occurring in Li_2CdGeS_4 span from 106.3 (5) to 113.4 (5)°.

Pauling's fourth rule states that in materials containing different cations, those with higher valency and small coordination number tend not to share corners, edges, or faces in order to spread out highly charged centers (Pauling, 1929). Each of the Si-, Ge-, and Sn-centered tetrahedra are separated from each other in all of the I_2–II–IV–VI_4 structure types. However, the GeS_4 tetrahedra share a corner in $Li_4CdGe_2S_7$, to form a $[Ge_2S_7]^{6-}$ subunit (Fig. 3). This may be due to the stoichiometry of the I_4–II–IV_2–VI_7 compounds or proof that 'covalent and electronic-structure effects' may take precedence over electrostatic phenomena, as proposed by George and co-workers for materials that infringe upon Pauling's fourth rule (George *et al.*, 2020; Glenn *et al.*, 2021). It should be noted that the longest Ge—S distances are those where the corners are shared; S4 serves as the bridge for the two GeS_4 tetrahedra to form the $[Ge_2S_7]^{6-}$ subunit.

Table 4
Bond distances (Å) in $Li_4CdGe_2S_7$ and Li_2CdGeS_4.

$Li_4CdGe_2S_7$	Bond distance	Li_2CdGeS_4	Bond distance
Li1—S5	2.374 (10)	Li—S3	2.402 (9)
Li1—S2	2.408 (10)	Li—S1	2.41 (2)
Li1—S3	2.421 (10)	Li—S1	2.424 (7)
Li1—S4	2.559 (10)	Li—S2	2.446 (6)
Avg Li1—S	2.44 (2)	Avg Li—S	2.42 (2)
Li2—S1	2.380 (13)		
Li2—S5	2.401 (13)		
Li2—S7	2.437 (10)		
Li2—S6	2.447 (12)		
Avg Li2—S	2.42 (2)		
Li3—S3	2.385 (10)		
Li3—S1	2.420 (12)		
Li3—S2	2.428 (7)		
Li3—S7	2.440 (12)		
Avg Li3—S	2.42 (2)		
Li4—S5	2.392 (9)		
Li4—S3	2.397 (10)		
Li4—S6	2.428 (10)		
Li4—S4	2.567 (11)		
Avg Li4—S	2.45 (2)		
Avg Li—S	2.43 (4)		
Cd—S1	2.5235 (8)	Cd—S3	2.5204 (10)
Cd—S7	2.5440 (9)	Cd—S1	2.5493 (12)
Cd—S6	2.5487 (10)	Cd—S2	2.5568 (6)
Cd—S2	2.5575 (9)	Cd—S2	2.5568 (6)
Avg Cd—S	2.543 (2)	Avg Cd—S	2.546 (2)
Ge1—S3	2.1680 (8)	Ge—S3	2.2075 (14)
Ge1—S2	2.2055 (9)	Ge—S1	2.2099 (9)
Ge1—S1	2.2141 (8)	Ge—S2	2.2152 (6)
Ge1—S4	2.2862 (8)	Ge—S2	2.2152 (6)
Avg Ge1—S	2.218 (2)	Avg Ge—S	2.212 (2)
Ge2—S5	2.1577 (8)		
Ge2—S6	2.2024 (10)		
Ge2—S7	2.2045 (8)		
Ge2—S4	2.2926 (9)		
Avg Ge2—S	2.214 (2)		
Avg Ge—S	2.216 (2)		

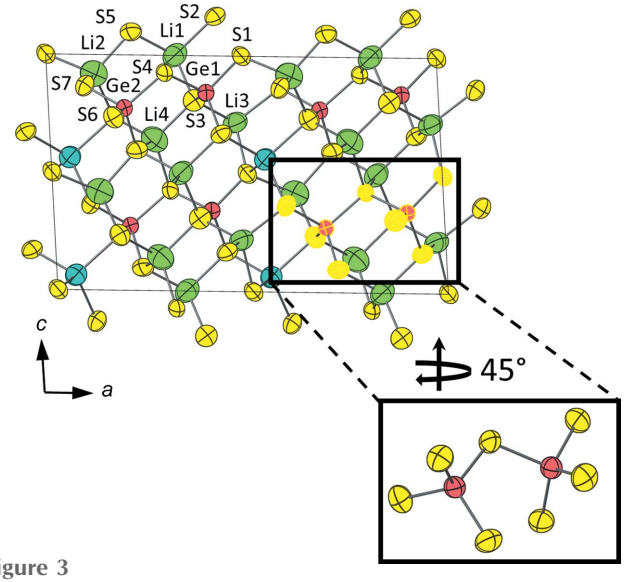

Figure 3
Displacement ellipsoid representation of $Li_4CdGe_2S_7$ drawn with 99% probability. Crystallographically unique atoms are labeled. Highlighted in the bottom right corner is one of the $[Ge_2S_7]^{6-}$ subunits.

s20532296, 2022, 9, Downloaded from https://onlinelibrary.wiley.com/doi/10.1107/S2053229622008014 by Missouri University Of Science, Wiley Online Library on [21/02/2023]. See the Terms and Conditions (https://onlinelibrary.wiley.com/terms-and-conditions) on Wiley Online Library for rules of use; OA articles are governed by the applicable Creative Commons License

Table 5
Bond angles (°) for $Li_4CdGe_2S_7$ and Li_2CdGeS_4.

$Li_4CdGe_2S_7$	Bond angle	Li_2CdGeS_4	Bond angle
S5—Li1—S2	107.5 (4)	S3—Li—S2	110.3 (4)
S5—Li1—S3	113.8 (4)	S3—Li—S1	107.9 (5)
S2—Li1—S3	109.5 (4)	S2—Li—S1	109.9 (5)
S5—Li1—S4	112.5 (4)	S3—Li—S2	106.3 (5)
S2—Li1—S4	106.8 (4)	S2—Li—S2	108.9 (5)
S3—Li1—S4	106.5 (4)	S1—Li—S2	113.4 (5)
Avg S—Li1—S	109 (1)	Avg S—Li—S	109 (1)
S1—Li2—S5	108.3 (5)		
S1—Li2—S7	106.0 (5)		
S5—Li2—S7	104.4 (4)		
S1—Li2—S6	113.3 (4)		
S5—Li2—S6	110.4 (5)		
S7—Li2—S6	114.0 (5)		
Avg S—Li1—S	109 (1)		
S3—Li3—S1	109.9 (4)		
S3—Li3—S2	113.8 (5)		
S1—Li3—S2	101.4 (3)		
S3—Li3—S7	110.0 (4)		
S1—Li3—S7	112.3 (5)		
S2—Li3—S7	109.3 (4)		
Avg S—Li1—S	109 (1)		
S5—Li4—S3	107.5 (4)		
S5—Li4—S6	111.9 (4)		
S3—Li4—S6	105.7 (4)		
S5—Li4—S4	110.0 (4)		
S3—Li4—S4	115.7 (4)		
S6—Li4—S4	106.1 (3)		
Avg S—Li1—S	109 (1)		
Avg S—Li—S	109 (2)		
S1—Cd—S7	112.35 (3)	S3—Cd—S1	110.32 (4)
S1—Cd—S6	112.75 (3)	S3—Cd—S2	110.10 (2)
S7—Cd—S6	105.41 (3)	S1—Cd—S2	108.14 (2)
S1—Cd—S2	110.77 (3)	S3—Cd—S2	110.10 (2)
S7—Cd—S2	109.69 (2)	S1—Cd—S2	108.14 (2)
S6—Cd—S2	105.52 (3)	S2—Cd—S2	110.01 (3)
Avg S—Cd—S	109.42 (7)	Avg S—Cd—S	109.47 (6)
S3—Ge1—S2	116.23 (3)		
S3—Ge1—S1	112.82 (3)		
S2—Ge1—S1	107.87 (3)		
S3—Ge1—S4	110.03 (3)		
S2—Ge1—S4	106.82 (3)		
S1—Ge1—S4	101.95 (3)		
Avg S—Ge1—S	109.29 (7)		
S5—Ge2—S6	111.99 (3)	S3—Ge—S1	110.69 (5)
S5—Ge2—S7	109.20 (3)	S3—Ge—S2	108.64 (3)
S6—Ge2—S7	111.08 (3)	S1—Ge—S2	111.15 (3)
S5—Ge2—S4	111.93 (3)	S3—Ge—S2	108.64 (3)
S6—Ge2—S4	104.90 (3)	S1—Ge—S2	111.15 (3)
S7—Ge2—S4	107.62 (3)	S2—Ge—S2	106.43 (4)
Avg S—Ge2—S	109.5 (5)	Avg S—Ge—S	109.45 (9)
Avg S—Ge—S	109.4 (5)		

Minimum bounding ellipsoid (MBE) analysis of the coordination environments for the ions within $Li_4CdGe_2S_7$ and Li_2CdGeS_4 was carried out using the PIEFACE (Polyhedral-Inscribing Ellipsoids for Analyzing Crystallographic Environments) software package (Cumby & Attfield, 2017). With this method, the smallest ellipsoid volume that encompasses all atoms within the coordination polyhedron is analyzed for distortions (Table 6). The center displacements for the metal ions are larger in the title compound. In $Li_4CdGe_2S_7$, the D value for Cd is ∼3× and for Ge ∼2–3× those of the corresponding ions in Li_2CdGeS_4. Upon comparison of the $\sigma(R)$ values in both diamond-like compounds, it is evident that the values in $Li_4CdGe_2S_7$ are greater on average, indicating that there is more tetrahedral distortion in this compound, as one would anticipate bearing in mind Pauling's second rule.

In order to further evaluate the structure of $Li_4CdGe_2S_7$, the bond valence sums (BVSs) and global instability index (G) values were calculated. BVS calculations relate the bond length and bond valence through Equation (3).

$$\mathrm{BVS} = \sum_j s_{ij};\ s_{ij} = \exp\left[\left(r_0 - r_{ij}\right)/b\right] \qquad (3)$$

In this equation, the term s_{ij} refers to the individual bond valences, r_0 is a constant for the cation–anion pair of interest, r_{ij} is the experimentally determined bond distance between ions i and j, and b is an empirically determined constant that is often found to be 0.37 Å, as is the case for the bonds present in the title compound (Brown & Altermatt, 1985; Brown, 1992; O'Keeffe, 1990). There is good agreement between the calculated BVSs and expected oxidation states for the ions in $Li_4CdGe_2S_7$, as well as those in Li_2CdGeS_4, which have been included for the purpose of comparison (Table 7).

The differences between the BVSs and expected oxidation states can be analyzed through the calculation of G values. This value helps to quantify the extent to which the valence sum rule is 'violated' throughout the entirety of the structure (Brown & Altermatt, 1985; Salinas-Sanchez *et al.*, 1992). This metric is calculated through Equation (4), where V_i is the expected valence of the particular ion and N represents the number of ions in the formula unit.

$$G = \sqrt{\frac{\sum_{i=1}^{N}(\mathrm{BVS} - V_i)^2}{N}} \qquad (4)$$

Using two slightly dissimilar r_0 for the Cd—S bond that are provided by two different sources, the two G values calculated for both $Li_4CdGe_2S_7$ and Li_2CdGeS_4, 0.08 (or 0.09) and 0.07 (or 0.09), respectively, are well within the range indicative of reasonable structural strain ($0.05 < G < 0.2$) (Table 7). These values are lower than those calculated for similar compounds reported by our group, for example, $Cu_4ZnGe_2Se_7$, Cu_2MnGeS_4, and $Cu_4MnGe_2S_7$, which range from 0.16 to 0.20 (Sinagra *et al.*, 2021; Glenn *et al.*, 2021). These results, in addition to the excellent refinement statistics of the single-crystal structure, give us confidence in our structure solution and refinement for the title compound.

3.2. Powder X-ray diffraction

Powder X-ray diffraction data indicate that $Li_4CdGe_2S_7$ was prepared as the major phase of the reaction product (Fig. 4). The I_2–II–IV–VI_4 analog, namely Li_2CdGeS_4, is also present in a significant amount (Lekse *et al.*, 2009). Future work will involve optimizing the synthetic process necessary to achieve the phase-pure $Li_4CdGe_2S_7$ that will be needed for further NLO characterization. Several attempts to optimize the synthetic procedure were carried out, including the use of

s20532296, 2022, 9, Downloaded from https://onlinelibrary.wiley.com/doi/10.1107/S2053229622008014 by Missouri University Of Science, Wiley Online Library on [21/02/2023]. See the Terms and Conditions (https://onlinelibrary.wiley.com/terms-and-conditions) on Wiley Online Library for rules of use; OA articles are governed by the applicable Creative Commons License

Table 6
PIEFACE ellipsoid data (Å) for $Li_4CdGe_2S_7$ (top) and Li_2CdGeS_4 (bottom)†.

Atom	*R*1	*R*2	*R*3	<*R*>	$\sigma(R)$	*S*	*D*	Coordination number
Li1	2.533	2.433	2.350	2.439	0.075	0.005	0.094	4
Li2	2.538	2.375	2.326	2.413	0.091	0.044	0.088	4
Li3	2.529	2.438	2.278	2.415	0.104	−0.029	0.079	4
Li4	2.596	2.444	2.290	2.444	0.125	−0.005	0.049	4
Cd	2.616	2.552	2.456	2.541	0.066	−0.013	0.088	4
Ge1	2.285	2.215	2.139	2.213	0.060	−0.004	0.145	4
Ge2	2.283	2.201	2.155	2.213	0.053	0.015	0.076	4
S1	2.524	2.338	2.227	2.363	0.122	0.026	0.317	4
S2	2.556	2.353	2.279	2.396	0.117	0.048	0.141	4
S3	2.418	2.332	2.265	2.338	0.062	0.006	0.169	4
S4	2.552	2.452	2.264	2.423	0.119	−0.037	0.147	4
S5	2.434	2.314	2.224	2.324	0.086	0.010	0.192	4
S6	2.500	2.363	2.332	2.399	0.073	0.042	0.221	4
S7	2.532	2.366	2.301	2.400	0.097	0.038	0.189	4
Li	2.493	2.424	2.338	2.418	0.063	−0.008	0.038	4
Cd	2.565	2.553	2.519	2.546	0.020	−0.008	0.032	4
Ge	2.256	2.205	2.173	2.211	0.034	0.008	0.044	4
S1	2.476	2.381	2.325	2.394	0.062	0.015	0.219	4
S2	2.500	2.382	2.326	2.403	0.072	0.024	0.162	4
S3	2.413	2.390	2.317	2.373	0.041	−0.021	0.233	4

† *R*1, *R*2, and *R*3 are the radii of the ellipsoids, <*R*> is the average ellipsoid radius, $\sigma(R)$ is the polyhedral distortion, *S* is the shape parameter, and *D* is the center displacement, which shows the atom displacement relative to the center of the ellipsoid.

different maximum holding temperatures (750, 800, and 850 °C), various holding times at high temperature (3, 5, and 7 d), and the addition of excess Li_2S (10 and 20%). As none of these conditions have yielded a phase-pure product, it seems that the ideal synthetic procedure will require the simultaneous tuning of multiple synthetic parameters, which may necessitate a significant amount of time.

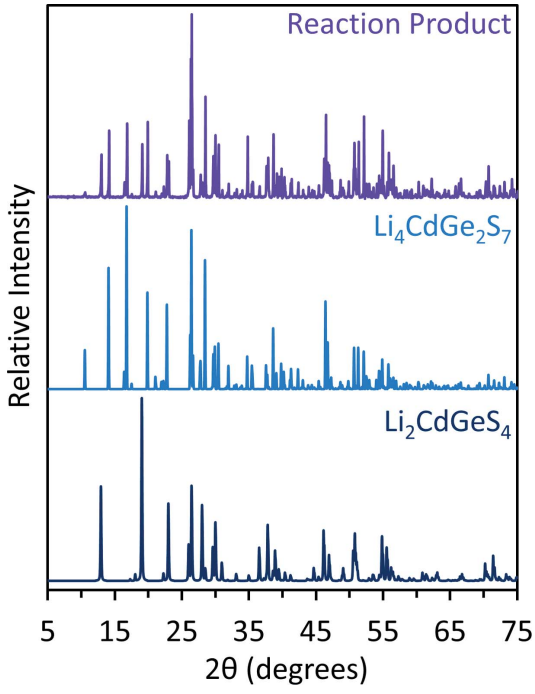

Figure 4
Laboratory-grade powder X-ray pattern of the reaction product targeting $Li_4CdGe_2S_7$ compared to the calculated patterns of $Li_4CdGe_2S_7$ and Li_2CdGeS_4.

3.3. Optical bandgap

The diffuse reflectance spectrum for a microcrystalline sample of $Li_4CdGe_2S_7$ was converted to absorption and plotted as a function of energy. The optical bandgap, E_g, of the title compound was estimated to be ~3.6 eV, corresponding to ~345 nm in the ultraviolet region and correlating with the colorless nature of the crystals (see Fig. 5). The presence of both the I_4–II–IV_2–VI_7 and I_2–II–IV–VI_4 phases can be seen in the absorption edge, with the latter becoming apparent in the tail region of the absorption edge with a bandgap of

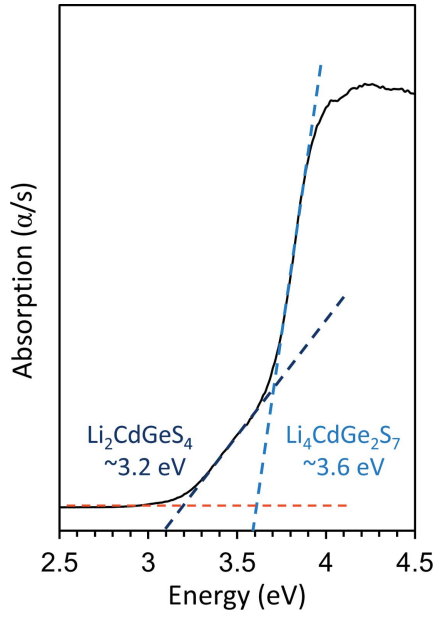

Figure 5
Optical diffuse reflectance spectrum converted to absorption for $Li_4CdGe_2S_7$.

s20532296, 2022, 9, Downloaded from https://onlinelibrary.wiley.com/doi/10.1107/S2053229622008014 by Missouri University Of Science, Wiley Online Library on [21/02/2023]. See the Terms and Conditions (https://onlinelibrary.wiley.com/terms-and-conditions) on Wiley Online Library for rules of use; OA articles are governed by the applicable Creative Commons License

~3.2 eV (Fig. 5). This value agrees well with the value of 3.15 eV previously reported by our group for phase-pure samples of Li_2CdGeS_4 (Brant *et al.*, 2015). This spectrum also suggests that $Li_4CdGe_2S_7$ is the major phase.

3.4. NLO

Fig. 6(*a*) shows the SHG counts measured from the reference (black) and the title compound (red) at λ = 1.8 µm, where the SHG counts were averaged for the sieved AGS specimen prepared with eight different particle size ranges. It is not possible to reliably estimate the SHG coefficient of $Li_4CdGe_2S_7$, because PM was not determined. Nonetheless, this early result indicates that the compound's SHG coefficient should be comparable to that of the reference. It was found that the title compound exhibits a stronger SHG response in the visible range, compared with that of the reference, because the latter undergoes bandgap absorption of SHG at this wavelength. The excellent SHG performance of our sample across the entire visible spectrum is well demonstrated by Fig. 6(*c*), showing the color change of SHG radiation from the sample when λ was tuned from 1.0 to 1.3 µm with increments of 0.1 µm.

The intensity-dependent SHG counts (dots) for $Li_4CdGe_2S_7$ are plotted in Fig. 6(*b*), in which the ideal square-law case, *i.e.* when no laser-induced damage occurs, corresponds to the red dashed line. It was found that the data points start to deviate from the line representing the ideal case when the input intensity exceeds 10 GW cm^{-2}. This highly impressive LIDT, which is more than an order of magnitude greater than that of AGS, is likely due, at least in part, to the wide optical bandgap of the title compound, ~3.6 eV, which is far wider than the bandgap of 2.6 eV observed for AGS (Catella & Burlage, 1998).

We were not able to estimate the three-photon absorption coefficient as the sample was ungraded; however, the data seem to indicate the case for saturable absorption, a phenomenon that we have also observed for other diamond-like compounds (Zhang, Stoyko *et al.*, 2020; Glenn *et al.*, 2021). For example, Cu_2MnGeS_4 (Glenn *et al.*, 2021), $Li_4CdSn_2S_7$ (Zhang, Stoyko *et al.*, 2020), and Li_2CdGeS_4 (Jang *et al.*, 2014) have also been found to exhibit saturable absorption. It should be noted that the LIDT for $Li_4CdGe_2S_7$ is much greater than that of the analogous I_2–II–IV–VI_4 phase Li_2CdGeS_4 (Jang *et al.*, 2014), and would likely be even higher when prepared in a phase-pure form.

3.5. Electronic structure calculations

The calculated electronic band diagram for $Li_4CdGe_2S_7$ is displayed on the left-hand side of Fig. 7. The dispersion of the bands along the high-symmetry points in the Brillouin zone (Fig. 7) indicates the direct nature of the bandgap. The top of the valence and bottom of the conduction band occur at the Γ point. The calculated band gap of 2.55 eV represents the wide-bandgap semiconductor nature of the compound. However,

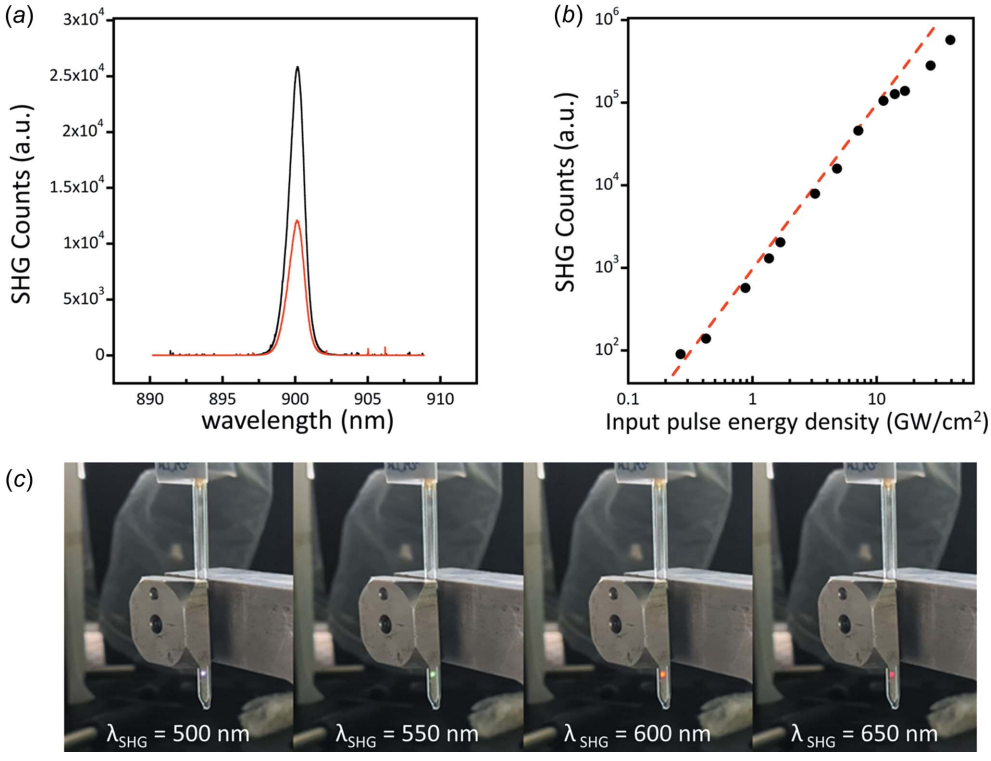

Figure 6
(*a*) Relative SHG counts from the reference (black) and $Li_4CdGe_2S_7$ (red). (*b*) SHG counts *versus* input intensity at 1.064 µm. The red line is the case for ideal SHG. (*c*) Representative photos, showing strong SHG signals from $Li_4CdGe_2S_7$ enclosed in the fused-silica tube over the visible range, when excited at λ = 1.0, 1.1, 1.2, and 1.3 µm, from left to right, respectively.

s20532296, 2022, 9, Downloaded from https://onlinelibrary.wiley.com/doi/10.1107/S2053229622008014 by Missouri University Of Science, Wiley Online Library on [21/02/2023]. See the Terms and Conditions (https://onlinelibrary.wiley.com/terms-and-conditions) on Wiley Online Library for rules of use; OA articles are governed by the applicable Creative Commons License

Table 7
Calculated BVSs and G values for $Li_4CdGe_2S_7$ and Li_2CdGeS_4.

Compound	Li^+ (avg)	Cd^{2+}	Ge^{4+} (avg)	S^{2-} (avg)	G
$Li_4CdGe_2S_7$†	1.07	1.96	4.04	2.05	0.08
$Li_4CdGe_2S_7$‡	1.07	2.10	4.04	2.07	0.09
Li_2CdGeS_4†	1.10	1.95	4.06	2.06	0.07
Li_2CdGeS_4‡	1.10	2.08	4.06	2.09	0.09

† Cd—S r_0 value from Brown & Altermatt (1985). ‡ Cd—S r_0 value from Palenik (2006).

the bandgap is underestimated as is usually the case for bandgap determination by conventional DFT methods (Nakamura *et al.*, 2010; Chen & Ravindra, 2013; Khyzhun *et al.*, 2015; Choi *et al.*, 2015). The calculated projected density of states (DOS) showing the different atomic orbital contributions for $Li_4CdGe_2S_7$ is shown on the right-hand side of Fig. 7. The states below the Fermi level, E_F, at the top of the valence band are dominated by bands with S 3*p* character; smaller contributions arising from bands of Cd 4*d* and 4*p*, Li 2*s*, and Ge 4*p* character can also be discerned (Fig. 7). The conduction band minimum is mainly comprised of bands with S 3*p* and Ge 4*s* character, most likely arising from the Ge—S antibonding states, and smaller contributions from the Cd *p*. Qualitatively, there is a close agreement between the calculated electronic structure of $Li_4CdGe_2S_7$ compared to that reported for Li_2CdGeS_4.

4. Conclusion

$Li_4CdGe_2S_7$ and Li_2CdGeS_4 have qualitatively similar electronic structures and crystal structures that can be considered derivatives of lonsdaleite. The differences between the two compounds lie in the increased tetrahedral distortions found in $Li_4CdGe2S_7$ and the wider optical bandgap that seemingly leads to enhanced IR–NLO performance. The SHG and LIDT measurements indicate that $Li_4CdGe_2S_7$ is among the front runners as an excellent candidate for IR–NLO devices. Based on the large LIDT demonstrated here, $Li_4CdGe_2S_7$ would be very useful in high-powered laser applications. Further synthetic efforts are currently underway to prepare $Li_4CdGe_2S_7$ as a phase-pure microcrystalline powder and as sizeable single crystals to more precisely assess the NLO properties of this material. Based on the results presented here, as well as those previously reported for $Li_4CdSn_2S_7$, other lithium-containing I_4–II–IV_2–VI_7 compounds should be pursued for their IR–NLO properties.

Acknowledgements

JAA, SSS and AJC acknowledge the support of the National Science Foundation of the United States. JIJ acknowledges support from the Basic Science Research Program through the National Research Foundation of Korea (NRF), funded by the Korean government. AC and SB acknowledge the National Science Foundation of the United States for funding. The authors gratefully acknowledge Gooch and Housego (Ohio) LLC for providing the optical-quality commercial-grade $AgGaS_2$ and $AgGaSe_2$ single-crystal reference materials. A special thanks goes to Gary Catella for inspiration and help with obtaining the commercial-grade samples. JAA thanks the late Professor Erwin Parthé for fruitful discussions and encouragement.

Funding information

Funding for this research was provided by: National Science Foundation of the United States (grant No. DMR-1611198 to JAA; grant No. DMR-1809128 to AJC and SB); National Research Foundation of Korea (grant No. 2021R1A2C2013625 to JIJ).

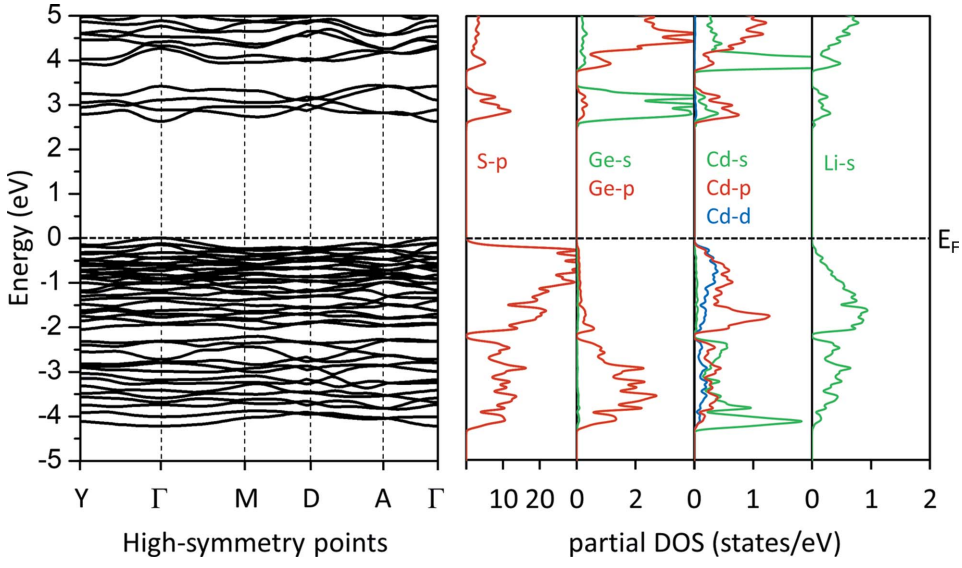

Figure 7
Electronic band structure and partial density of states (DOS) plotted from left to right for $Li_4CdGe_2S_7$. The Fermi level is indicated as E_F.

s20532296, 2022, 9, Downloaded from https://onlinelibrary.wiley.com/doi/10.1107/S2053229622008014 by Missouri University Of Science, Wiley Online Library on [21/02/2023]. See the Terms and Conditions (https://onlinelibrary.wiley.com/terms-and-conditions) on Wiley Online Library for rules of use; OA articles are governed by the applicable Creative Commons License

References

Abudurusuli, A., Huang, J., Wang, P., Yang, Z., Pan, S. & Li, J. (2021). *Angew. Chem. Int. Ed.* **60**, 24131–24136.

Aitken, J. A. (2001). PhD thesis, Michigan State University, Ann Arbor, USA.

Brant, J. A., Devlin, K. P., Bischoff, C., Watson, D., Martin, S. W., Gross, M. D. & Aitken, J. A. (2015). *Solid State Ionics*, **278**, 268–274.

Breithaupt, J. F. A. & Plattner, C. F. (1850). *Ann. Phys.* **80**, 383–391.

Brown, I. D. (1992). *Z. Kristallogr.* **199**, 255–272.

Brown, I. D. & Altermatt, D. (1985). *Acta Cryst.* B**41**, 244–247.

Bruker (2010). *APEX2* and *SMART*. Bruker AXS Inc., Madison, Wisconsin, USA.

Brunetta, C. D., Minsterman, W. C., Lake, C. H. & Aitken, J. A. (2012). *J. Solid State Chem.* **187**, 177–185.

Bundy, F. P. & Kasper, J. S. (1967). *J. Chem. Phys.* **46**, 3437–3446.

Catella, G. C. & Burlage, D. (1998). *MRS Bull.* **23**, 28–36.

Chen, D. & Ravindra, N. M. (2013). *J. Alloys Compd.* **579**, 468–472.

Cheng, X., Whangbo, M.-H., Hong, M. & Deng, S. (2019). *Inorg. Chem.* **58**, 9572–9575.

Choi, S. G., Park, J. S., Donohue, A. L., Christensen, S. T., To, B., Beall, C., Wei, S. H. & Repins, I. L. (2015). *Phys. Rev. Appl.* **4**, 054006.

Craig, A. J., Stoyko, S. S., Bonnoni, A. & Aitken, J. A. (2020). *Acta Cryst.* E**76**, 1117–1121.

Cumby, J. & Attfield, J. P. (2017). *Nat. Commun.* **8**, 14235.

Degen, T., Sadki, M., Bron, E., König, U. & Nénert, G. (2014). *Powder Diffr.* **29** (Suppl. S2), S13–S18.

Dogguy, M., Jaulmes, S., Laruelle, P. & Rivet, J. (1982). *Acta Cryst.* B**38**, 2014–2016.

Flack, H. D. & Bernardinelli, G. (1999). *Acta Cryst.* A**55**, 908–915.

Friedel, C. (1861). *C. R. Acad. Sci. Paris*, pp. 983–985.

Frondel, C. & Marvin, U. B. (1967). *Nature*, **214**, 587–589.

George, J., Waroquiers, D., Di Stefano, D., Petretto, G., Rignanese, G.-M. & Hautier, G. (2020). *Angew. Chem. Int. Ed.* **59**, 7569–7575.

Giannozzi, P., Baroni, S., Bonini, N., Calandra, M., Car, R., Cavazzoni, C., Ceresoli, D., Chiarotti, G. L., Cococcioni, M., Dabo, I., Dal Corso, A., de Gironcoli, S., Fabris, S., Fratesi, G., Gebauer, R., Gerstmann, U., Gougoussis, C., Kokalj, A., Lazzeri, M., Martin-Samos, L., Marzari, N., Mauri, F., Mazzarello, R., Paolini, S., Pasquarello, A., Paulatto, L., Sbraccia, C., Scandolo, S., Sclauzero, G., Seitsonen, A. P., Smogunov, A., Umari, P. & Wentzcovitch, R. M. (2009). *J. Phys. Condens. Matter*, **21**, 395502.

Glenn, J. R., Cho, J. B., Wang, Y., Craig, A. J., Zhang, J.-H., Cribbs, M., Stoyko, S. S., Rosello, K. E., Barton, C., Bonnoni, A., Grima-Gallardo, P., MacNeil, J. H., Rondinelli, J. M., Jang, J. I. & Aitken, J. A. (2021). *Dalton Trans.* **50**, 17524–17537.

Goryunova, N. A. (1965). In *The Chemistry of Diamond-like Semiconductors*. Cambridge, MA: Massachusetts Insitute of Technology.

Gulay, L. D., Olekseyuk, I. D. & Parasyuk, O. V. (2002). *J. Alloys Compd.* **340**, 157–166.

Guo, Y., Liang, F., Li, Z., Xing, W., Lin, Z., Yao, J. & Wu, Y. (2019). *Cryst. Growth Des.* **19**, 5494–5497.

Hough, R. M., Gilmour, I., Pillinger, C. T., Arden, J. W., Gilkess, K. W. R., Yuan, J. & Milledge, H. J. (1995). *Nature*, **378**, 41–44.

Huang, Y., Wu, K., Cheng, J., Chu, Y., Yang, Z. & Pan, S. (2019). *Dalton Trans.* **48**, 4484–4488.

Jackson, A. G., Ohmer, M. C. & LeClair, S. R. (1997). *Infrared Phys. Technol.* **38**, 233–244.

Jang, J. I., Clark, D. J., Brant, J. A., Aitken, J. A. & Kim, Y. S. (2014). *Opt. Lett.* **39**, 4579–4582.

Kaib, T., Haddadpour, S., Andersen, H. F., Mayrhofer, L., Järvi, T. T., Moseler, M., Möller, K.-C. & Dehnen, S. (2013). *Adv. Funct. Mater.* **23**, 5693–5699.

Khyzhun, O. Y., Bekenev, V. L., Ocheretova, V. A., Fedorchuk, A. O. & Parasyuk, O. V. (2015). *Physica B*, **461**, 75–84.

Kraus, D., Ravasio, A., Gauthier, M., Gericke, D. O., Vorberger, J., Frydrych, S., Helfrich, J., Fletcher, L. B., Schaumann, G., Nagler, B., Barbrel, B., Bachmann, B., Gamboa, E. J., Göde, S., Granados, E., Gregori, G., Lee, H. J., Neumayer, P., Schumaker, W., Döppner, T., Falcone, R. W., Glenzer, S. H. & Roth, M. (2016). *Nat. Commun.* **7**, 10970.

Kubelka, P. & Munk, F. (1931). *Ein Beitrag zur Optik von Farbanstrichen*. *Z. Techn. Phys.* **12**, 593–601.

Lekse, J. W., Moreau, M. A., McNerny, K. L., Yeon, J., Halasyamani, P. S. & Aitken, J. A. (2009). *Inorg. Chem.* **48**, 7516–7518.

Monkhorst, H. J. & Pack, J. D. (1976). *Phys. Rev. B*, **13**, 5188–5192.

Nakamura, S., Maeda, T. & Wada, T. (2010). *Jpn. J. Appl. Phys.* **49**, 121203.

O'Keeffe, M. (1990). *Acta Cryst.* A**46**, 138–142.

Palenik, G. J. (2006). *Can. J. Chem.* **84**, 99–104.

Palmer, D. (2019). *CrystalMaker*. CrystalMaker Software Ltd, Yarnton, Oxfordshire, England. http://crystalmaker.com/.

Pamplin, B. (1981). *Prog. Cryst. Growth Charact.* **3**, 179–192.

Parasyuk, O. V., Romanyuk, Y. E. & Olekseyuk, I. D. (2005). *J. Cryst. Growth*, **275**, e159–e162.

Parthé, E. (1964). In *Crystal Chemistry of Tetrahedral Structures*. New York, NY: Gordon and Breach Science Publishers, Inc.

Parthé, E. (1996). In *Elements of Inorganic Structural Chemistry: Selected Efforts to Predict Structural Features*, 2nd ed. Geneva: K. Sutter Parthé.

Pauling, L. (1929). *J. Am. Chem. Soc.* **51**, 1010–1026.

Pauling, L. & Weinbaum, S. (1934). *Z. Kristallogr.* **88**, 48–53.

Perdew, J. P., Burke, K. & Ernzerhof, M. (1996). *Phys. Rev. Lett.* **77**, 3865–3868.

Perdew, J. P., Ruzsinszky, A., Csonka, G. I., Vydrov, O. A., Scuseria, G. E., Constantin, L. A., Zhou, X. & Burke, K. (2008). *Phys. Rev. Lett.* **100**, 136406.

Salinas-Sanchez, A., Garcia-Muñoz, J. L., Rodriguez-Carvajal, J., Saez-Puche, R. & Martinez, J. L. (1992). *J. Solid State Chem.* **100**, 201–211.

Schäfer, W., Scheunemann, K. & Nitsche, R. (1980). *Mater. Res. Bull.* **15**, 933–937.

Sheldrick, G. M. (2002). *SADABS*. University of Göttingen, Germany.

Sheldrick, G. M. (2015*a*). *Acta Cryst.* A**71**, 3–8.

Sheldrick, G. M. (2015*b*). *Acta Cryst.* C**71**, 3–8.

Sinagra, C. W., Saouma, F. O., Otieno, C. O., Lapidus, S. H., Zhang, J.-H., Craig, A. J., Grima-Gallardo, P., Brant, J. A., Rosmus, K. A., Rosello, K. E., Jang, J. I. & Aitken, J. A. (2021). *J. Alloys Compd.* **888**, 161499.

Smith, D. K. & Jenkins, R. (1996). *J. Res. Natl Inst. Stand. Technol.* **101**, 259–271.

Ulrich, F. & Zachariasen, W. (1925). *Z. Kristallogr. Cryst. Mater.* **62**, 260–273.

Wu, K., Yang, Z. & Pan, S. (2017). *Chem. Commun.* **53**, 3010–3013.

Zhang, J.-H., Clark, D. J., Brant, J. A., Rosmus, K. A., Grima, P., Lekse, J. W., Jang, J. I. & Aitken, J. A. (2020). *Chem. Mater.* **32**, 8947–8955.

Zhang, J.-H., Stoyko, S. S., Craig, A. J., Grima, P., Kotchey, J. W., Jang, J. I. & Aitken, J. A. (2020). *Chem. Mater.* **32**, 10045–10054.

s20532296, 2022, 9, Downloaded from https://onlinelibrary.wiley.com/doi/10.1107/S2053229622008014 by Missouri University Of Science, Wiley Online Library on [21/02/2023]. See the Terms and Conditions (https://onlinelibrary.wiley.com/terms-and-conditions) on Wiley Online Library for rules of use; OA articles are governed by the applicable Creative Commons License

supporting information

Acta Cryst. (2022). C**78**, 470-480 [https://doi.org/10.1107/S2053229622008014]

Crystal structure, electronic structure, and optical properties of the novel $Li_4CdGe_2S_7$, a wide-bandgap quaternary sulfide with a polar structure derived from lonsdaleite

Andrew J. Craig, Seung Han Shin, Jeong Bin Cho, Srikanth Balijapelly, Jordan C. Kelly, Stanislav S. Stoyko, Amitava Choudhury, Joon I. Jang and Jennifer A. Aitken

Computing details

Data collection: *APEX2* (Bruker, 2010); cell refinement: *SMART* (Bruker, 2010); data reduction: *SMART* (Bruker, 2010); program(s) used to solve structure: SHELXT (Sheldrick, 2015a); program(s) used to refine structure: *SHELXL2018* (Sheldrick, 2015b); molecular graphics: *CrystalMaker* (Palmer, 2019); software used to prepare material for publication: *SHELXL2018* (Sheldrick, 2015b).

Tetralithium cadmium digermanium heptasulfide

Crystal data

$Li_4CdGe_2S_7$
M_r = 509.76
Monoclinic, *Cc*
a = 16.8354 (10) Å
b = 6.7870 (4) Å
c = 10.1499 (6) Å
β = 93.710 (3)°
V = 1157.32 (12) Å^3
Z = 4
F(000) = 944
D_x = 2.926 Mg m^{-3}
Mo $K\alpha$ radiation, λ = 0.71073 Å
Cell parameters from 7524 reflections
θ = 2.4–33.0°
μ = 8.18 mm^{-1}
T = 293 K
Polyhedra, colourless
0.21 × 0.12 × 0.11 mm

Data collection

Bruker SMART APEXII diffractometer
φ and ω scan
Absorption correction: multi-scan (SADABS; Sheldrick, 2002)
T_{min} = 0.549, T_{max} = 0.747
7415 measured reflections
2634 independent reflections
2612 reflections with $I > 2\sigma(I)$
R_{int} = 0.017
θ_{max} = 27.5°, θ_{min} = 2.4°
$h = -21 \rightarrow 21$
$k = -8 \rightarrow 8$
$l = -13 \rightarrow 13$

Refinement

Refinement on F^2
Least-squares matrix: full
$R[F^2 > 2\sigma(F^2)]$ = 0.010
$wR(F^2)$ = 0.024
S = 1.08
2634 reflections
129 parameters
2 restraints
$w = 1/[\sigma^2(F_o^2) + (0.0097P)^2 + 0.0293P]$ where $P = (F_o^2 + 2F_c^2)/3$
$(\Delta/\sigma)_{max}$ = 0.001
$\Delta\rho_{max}$ = 0.27 e Å^{-3}
$\Delta\rho_{min}$ = −0.21 e Å^{-3}

s20532296, 2022, 9, Downloaded from https://onlinelibrary.wiley.com/doi/10.1107/S2053229622008014 by Missouri University Of Science, Wiley Online Library on [21/02/2023]. See the Terms and Conditions (https://onlinelibrary.wiley.com/terms-and-conditions) on Wiley Online Library for rules of use; OA articles are governed by the applicable Creative Commons License

Extinction correction: SHELXL2018 (Sheldrick, 2015b), $Fc^{*}=kFc[1+0.001xFc^{2}\lambda^{3}/\sin(2\theta)]^{-1/4}$
Extinction coefficient: 0.00183 (7)

Absolute structure: Refined as an inversion twin.
Absolute structure parameter: 0.001 (5)

Special details

Geometry. All esds (except the esd in the dihedral angle between two l.s. planes) are estimated using the full covariance matrix. The cell esds are taken into account individually in the estimation of esds in distances, angles and torsion angles; correlations between esds in cell parameters are only used when they are defined by crystal symmetry. An approximate (isotropic) treatment of cell esds is used for estimating esds involving l.s. planes.

Refinement. Refined as a 2-component inversion twin.

Fractional atomic coordinates and isotropic or equivalent isotropic displacement parameters (Å²)

	x	*y*	*z*	U_{iso}*/U_{eq}
Li1	0.3309 (6)	0.1842 (15)	0.5012 (10)	0.0224 (18)
Li2	0.1207 (8)	0.3276 (14)	0.4190 (13)	0.025 (2)
Li3	0.9764 (7)	0.3297 (11)	0.7180 (11)	0.0199 (19)
Li4	0.7674 (6)	0.1619 (14)	0.6423 (10)	0.025 (2)
Cd	0.54849 (2)	0.36329 (3)	0.56327 (4)	0.01770 (6)
Ge1	0.40538 (2)	0.33494 (7)	0.84280 (2)	0.01042 (11)
Ge2	0.19465 (2)	0.17688 (7)	0.77467 (2)	0.01045 (10)
S1	0.50089 (4)	0.29460 (12)	0.00091 (8)	0.01425 (15)
S2	0.43895 (5)	0.16838 (12)	0.66829 (7)	0.01398 (16)
S3	0.37399 (5)	0.35832 (12)	0.31017 (8)	0.01570 (17)
S4	0.30151 (5)	0.16992 (11)	0.92654 (7)	0.01258 (16)
S5	0.22120 (5)	0.33369 (13)	0.59790 (8)	0.01651 (18)
S6	0.66610 (5)	0.36507 (11)	0.73450 (8)	0.01491 (16)
S7	0.09614 (4)	0.32632 (13)	0.86708 (8)	0.01446 (16)

Atomic displacement parameters (Å²)

	U^{11}	U^{22}	U^{33}	U^{12}	U^{13}	U^{23}
Li1	0.022 (4)	0.025 (4)	0.021 (3)	−0.001 (3)	0.006 (3)	−0.001 (3)
Li2	0.028 (4)	0.021 (4)	0.025 (4)	−0.002 (3)	0.000 (3)	0.001 (3)
Li3	0.021 (3)	0.023 (4)	0.016 (4)	0.000 (3)	0.004 (3)	0.002 (3)
Li4	0.026 (4)	0.025 (4)	0.024 (4)	0.003 (3)	−0.003 (3)	−0.001 (3)
Cd	0.01709 (9)	0.01891 (11)	0.01720 (9)	0.00053 (13)	0.00176 (6)	0.00054 (13)
Ge1	0.00954 (19)	0.0111 (2)	0.01056 (18)	−0.00010 (12)	0.00062 (14)	−0.00022 (12)
Ge2	0.00921 (18)	0.01191 (19)	0.01018 (18)	−0.00051 (13)	0.00025 (13)	−0.00008 (13)
S1	0.0124 (3)	0.0164 (4)	0.0135 (3)	−0.0005 (3)	−0.0020 (2)	0.0005 (3)
S2	0.0160 (3)	0.0138 (4)	0.0124 (3)	−0.0002 (3)	0.0032 (3)	−0.0021 (3)
S3	0.0179 (4)	0.0117 (4)	0.0175 (4)	−0.0012 (3)	0.0018 (3)	−0.0008 (3)
S4	0.0098 (3)	0.0163 (4)	0.0115 (3)	−0.0024 (3)	−0.0002 (3)	0.0023 (3)
S5	0.0173 (4)	0.0203 (4)	0.0120 (4)	−0.0021 (3)	0.0011 (3)	0.0036 (3)
S6	0.0150 (4)	0.0124 (4)	0.0171 (3)	−0.0010 (3)	−0.0013 (3)	−0.0017 (3)
S7	0.0130 (4)	0.0146 (4)	0.0161 (3)	0.0020 (3)	0.0035 (3)	−0.0005 (3)

s20532296, 2022, 9, Downloaded from https://onlinelibrary.wiley.com/doi/10.1107/S2053229622008014 by Missouri University Of Science, Wiley Online Library on [21/02/2023]. See the Terms and Conditions (https://onlinelibrary.wiley.com/terms-and-conditions) on Wiley Online Library for rules of use; OA articles are governed by the applicable Creative Commons License

Geometric parameters (Å, º)

Li1—S5	2.374 (10)	Li4—S6	2.428 (10)
Li1—S2	2.408 (10)	Li4—S4^{ix}	2.567 (11)
Li1—S3	2.421 (10)	Cd—S1^{x}	2.5235 (8)
Li1—S4^{i}	2.559 (10)	Cd—S7^{ix}	2.5441 (9)
Li2—S1^{ii}	2.380 (13)	Cd—S6	2.5487 (10)
Li2—S5	2.401 (13)	Cd—S2	2.5576 (9)
Li2—S7^{iii}	2.437 (10)	Ge1—S3^{x}	2.1680 (8)
Li2—S6^{iv}	2.447 (12)	Ge1—S2	2.2055 (9)
Li3—S3^{v}	2.385 (10)	Ge1—S1^{xi}	2.2141 (8)
Li3—S1^{v}	2.420 (12)	Ge1—S4	2.2862 (8)
Li3—S2^{vi}	2.428 (7)	Ge2—S5	2.1577 (8)
Li3—S7^{vii}	2.440 (12)	Ge2—S6^{xii}	2.2024 (10)
Li4—S5^{viii}	2.393 (9)	Ge2—S7	2.2045 (8)
Li4—S3^{v}	2.397 (10)	Ge2—S4	2.2926 (9)
S5—Li1—S2	107.5 (4)	Ge1^{xiii}—S1—Li2^{ix}	112.5 (3)
S5—Li1—S3	113.8 (4)	Ge1^{xiii}—S1—Li3^{iv}	123.0 (3)
S2—Li1—S3	109.5 (4)	Li2^{ix}—S1—Li3^{iv}	113.2 (4)
S5—Li1—S4^{i}	112.5 (4)	Ge1^{xiii}—S1—Cd^{iii}	105.78 (3)
S2—Li1—S4^{i}	106.8 (4)	Li2^{ix}—S1—Cd^{iii}	98.4 (3)
S3—Li1—S4^{i}	106.5 (4)	Li3^{iv}—S1—Cd^{iii}	99.34 (19)
S1^{ii}—Li2—S5	108.3 (5)	Ge1—S2—Li1	108.8 (2)
S1^{ii}—Li2—S7^{iii}	106.0 (5)	Ge1—S2—Li3^{xii}	113.3 (3)
S5—Li2—S7^{iii}	104.4 (4)	Li1—S2—Li3^{xii}	111.3 (4)
S1^{ii}—Li2—S6^{iv}	113.2 (4)	Ge1—S2—Cd	107.38 (3)
S5—Li2—S6^{iv}	110.4 (5)	Li1—S2—Cd	102.5 (2)
S7^{iii}—Li2—S6^{iv}	114.0 (5)	Li3^{xii}—S2—Cd	113.0 (3)
S3^{v}—Li3—S1^{v}	109.9 (4)	Ge1^{iii}—S3—Li3^{iv}	113.5 (2)
S3^{v}—Li3—S2^{vi}	113.8 (5)	Ge1^{iii}—S3—Li4^{iv}	109.1 (2)
S1^{v}—Li3—S2^{vi}	101.4 (3)	Li3^{iv}—S3—Li4^{iv}	102.6 (4)
S3^{v}—Li3—S7^{vii}	110.0 (4)	Ge1^{iii}—S3—Li1	115.4 (2)
S1^{v}—Li3—S7^{vii}	112.3 (5)	Li3^{iv}—S3—Li1	108.3 (3)
S2^{vi}—Li3—S7^{vii}	109.3 (4)	Li4^{iv}—S3—Li1	107.0 (4)
S5^{viii}—Li4—S3^{v}	107.5 (4)	Ge1—S4—Ge2	109.01 (3)
S5^{viii}—Li4—S6	111.9 (4)	Ge1—S4—Li1^{xiv}	115.6 (2)
S3^{v}—Li4—S6	105.7 (4)	Ge2—S4—Li1^{xiv}	110.3 (2)
S5^{viii}—Li4—S4^{ix}	110.0 (4)	Ge1—S4—Li4^{ii}	108.5 (2)
S3^{v}—Li4—S4^{ix}	115.7 (4)	Ge2—S4—Li4^{ii}	110.8 (2)
S6—Li4—S4^{ix}	106.1 (3)	Li1^{xiv}—S4—Li4^{ii}	102.4 (4)
S1^{x}—Cd—S7^{ix}	112.35 (3)	Ge2—S5—Li1	110.0 (2)
S1^{x}—Cd—S6	112.75 (3)	Ge2—S5—Li4^{xv}	112.6 (3)
S7^{ix}—Cd—S6	105.41 (3)	Li1—S5—Li4^{xv}	102.9 (4)
S1^{x}—Cd—S2	110.77 (3)	Ge2—S5—Li2	116.5 (3)
S7^{ix}—Cd—S2	109.70 (2)	Li1—S5—Li2	102.1 (4)
S6—Cd—S2	105.52 (3)	Li4^{xv}—S5—Li2	111.3 (3)
S3^{x}—Ge1—S2	116.24 (3)	Ge2^{vi}—S6—Li4	117.8 (2)

s20532296, 2022, 9, Downloaded from https://onlinelibrary.wiley.com/doi/10.1107/S2053229622008014 by Missouri University Of Science, Wiley Online Library on [21/02/2023]. See the Terms and Conditions (https://onlinelibrary.wiley.com/terms-and-conditions) on Wiley Online Library for rules of use; OA articles are governed by the applicable Creative Commons License

S3^{x}—Ge1—S1^{xi}	112.82 (3)	Ge2^{vi}—S6—Li2^{v}	116.6 (2)
S2—Ge1—S1^{xi}	107.87 (3)	Li4—S6—Li2^{v}	104.7 (3)
S3^{x}—Ge1—S4	110.03 (3)	Ge2^{vi}—S6—Cd	106.34 (3)
S2—Ge1—S4	106.82 (3)	Li4—S6—Cd	105.6 (2)
S1^{xi}—Ge1—S4	101.95 (3)	Li2^{v}—S6—Cd	104.6 (3)
S5—Ge2—S6^{xii}	111.99 (3)	Ge2—S7—Li2^{x}	114.4 (3)
S5—Ge2—S7	109.20 (3)	Ge2—S7—Li3^{xvi}	110.8 (3)
S6^{xii}—Ge2—S7	111.08 (3)	Li2^{x}—S7—Li3^{xvi}	104.3 (4)
S5—Ge2—S4	111.93 (3)	Ge2—S7—Cd^{ii}	112.60 (3)
S6^{xii}—Ge2—S4	104.90 (3)	Li2^{x}—S7—Cd^{ii}	112.1 (3)
S7—Ge2—S4	107.62 (3)	Li3^{xvi}—S7—Cd^{ii}	101.6 (2)

Symmetry codes: (i) x, $-y$, $z-1/2$; (ii) $x-1/2$, $-y+1/2$, $z+1/2$; (iii) x, $-y+1$, $z-1/2$; (iv) $x-1/2$, $-y+1/2$, $z-1/2$; (v) $x+1/2$, $-y+1/2$, $z+1/2$; (vi) $x+1/2$, $y+1/2$, z; (vii) $x+1$, y, z; (viii) $x+1/2$, $y-1/2$, z; (ix) $x+1/2$, $-y+1/2$, $z-1/2$; (x) x, $-y+1$, $z+1/2$; (xi) x, y, $z+1$; (xii) $x-1/2$, $y-1/2$, z; (xiii) x, y, $z-1$; (xiv) x, $-y$, $z+1/2$; (xv) $x-1/2$, $y+1/2$, z; (xvi) $x-1$, y, z.

s20532296, 2022, 9, Downloaded from https://onlinelibrary.wiley.com/doi/10.1107/S2053229622008014 by Missouri University Of Science, Wiley Online Library on [21/02/2023]. See the Terms and Conditions (https://onlinelibrary.wiley.com/terms-and-conditions) on Wiley Online Library for rules of use; OA articles are governed by the applicable Creative Commons License